Microwave hyperspectral measurements for temperature and humidity atmospheric profiling from satellite: The clear-sky case

(article starts on next page)

RESEARCH ARTICLE

Correspondence to:
F. Aires,
filipe.aires@estellus.fr

Microwave hyperspectral measurements for temperature and humidity atmospheric profiling from satellite: The clear-sky case

Filipe Aires[1,2,3], Catherine Prigent[1,2], Emiliano Orlandi[4], Mathias Milz[5], Patrick Eriksson[6], Susanne Crewell[4], Chung-Chi Lin[7], and Ville Kangas[7]

[1]Estellus, Paris, France, [2]LERMA, Observatoire de Paris, Paris, France, [3]Water Center, Columbia University, New York, New York, USA, [4]Institute for Geophysics and Meteorology, University of Cologne, Cologne, Germany, [5]Department of Computer Science, Electrical and Space Engineering, LTU, Lulea, Sweden, [6]Global Environmental Measurements and Modeling, Chalmers University of Technology, Gothenburg, Sweden, [7]Earth Observation Projects Department, ESA, ESTEC, Noordwijk, Netherlands

Abstract This study investigates the benefits of a satellite HYperspectral Microwave Sensor (HYMS) for the retrieval of atmospheric temperature and humidity profiles, in the context of numerical weather prediction (NWP). In the infrared, hyperspectral instruments have already improved the accuracy of NWP forecasts. Microwave instruments so far only provide observations for a limited number of carefully selected channels. An information content analysis is conducted here to assess the impact of hyperspectral microwave measurements on the retrieval of temperature and water vapor profiles under clear-sky conditions. It uses radiative transfer simulations over a large variety of atmospheric situations. It accounts for realistic observation (instrument and radiative transfer) noise and for a priori information assumptions compatible with NWP practices. The estimated retrieval performance of the HYMS instrument is compared to those of the microwave instruments to be deployed on board the future generation of European operational meteorological satellites (MetOp-SG). The results confirm the positive impact of a HYMS instrument on the atmospheric profiling capabilities compared to MetOp-SG. Temperature retrieval uncertainty, compared to a priori information, is reduced by 2 to 10%, depending on the atmospheric height, and improvement rates are much higher than what will be obtained with MetOp-SG. For humidity sounding these improvements can reach 30%, a significant benefit as compared to MetOp-SG results especially below 250 hPa. The results are not very sensitive to the instrument noise, under our assumptions. The main impact provided by the hyperspectral information originates from the higher resolution in the O_2 band around 60 GHz. The results are presented over ocean at nadir, but similar conclusions are obtained for other incidence angles and over land.

1. Introduction

Passive microwave observations from satellites provide key information to numerical weather prediction (NWP) assimilation systems. Microwave measurements in the 50–60 GHz oxygen band for temperature sounding and in the 183 GHz water vapor line for humidity sounding have proven to be an important satellite contribution to NWP [*Cardinali*, 2009; *Radnoti et al.*, 2010; *Dee et al.*, 2011; *Lorenc and Marriott*, 2014]. The Advanced Microwave Sounding Unit (AMSU) A and B or the Microwave Humidity Sounder (MHS) on board the NOAA and EUMETSAT operational satellites allow for a significant reduction in the errors of the medium-range weather forecast. In addition, the microwave observations are increasingly used in cloudy and precipitating situations [*Bauer et al.*, 2010; *Geer*, 2013], where infrared (IR) observations only provide information on the atmosphere above the clouds.

The impact of the microwave observations on the quality of weather forecasts is high, despite the limited number of channels measured in the microwave (of the order of 20). NWP now benefits from infrared hyperspectral observations with instruments such as Atmospheric InfraRed Sounder, IASI (Infrared Atmospheric Sounding Interferometer), or Cross-Track Infrared Sounder, which contain several thousands of channels. A similar NWP impact of microwave instrument can be achieved with much less channels than these hyperspectral infrared instruments [*Cardinali*, 2009; *Radnoti et al.*, 2010; *Lorenc and Marriott*, 2014]. The hyperspectral information strongly improves the retrieval from infrared observations, and it could be expected that a better sampling
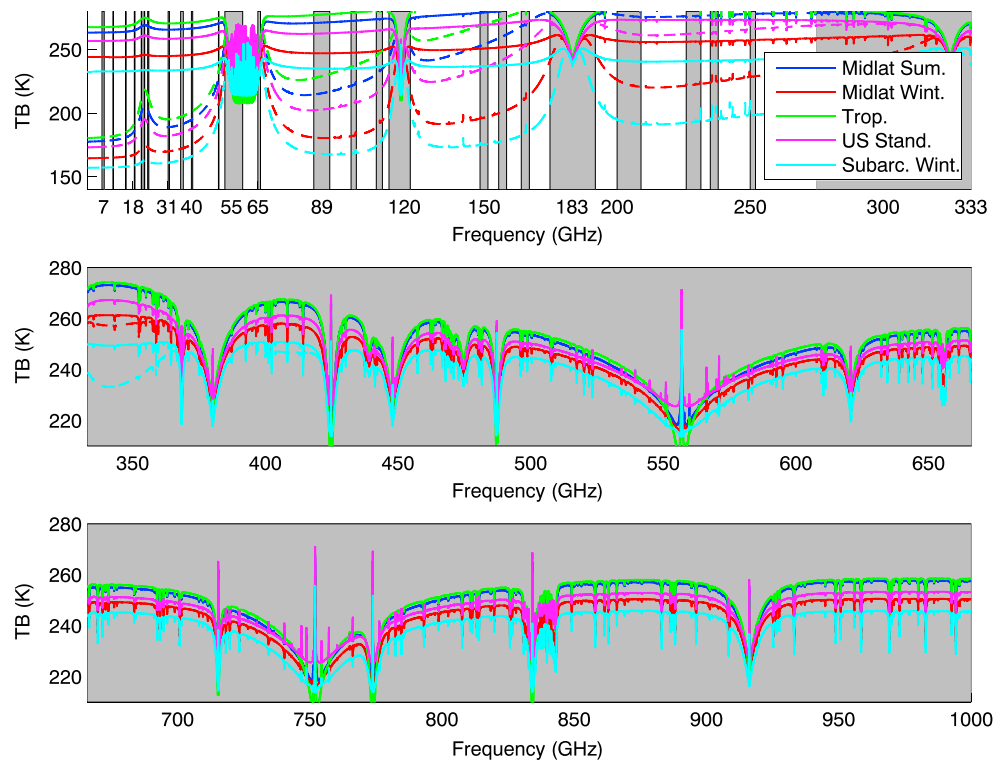
Figure 1. Simulated *TB*s from 1 to 1000 GHz, for a nadir view, for six atmospheric profiles (midlatitude summer, midlatitude winter, tropical, U.S. standard, and subarctic winter). The continuous lines correspond to simulations over land and the dashed lines over ocean. Grey regions are protected spectral bands [*Mellinger*, 2007] and include the bands that are fully protected (i.e., all emission prohibited), the ones that are rather well protected (i.e., intersatellite and satellite to fixed systems), and the ones that are shared with fixed systems but with a certain threshold defined. Above 275 GHz, the bands are not formally allocated yet (or at least were not when we enquired). They have been considered as protected in this study.

of the microwave spectrum would also help the microwave retrieval of temperature and water vapor profiles. Denser sampling along the absorption lines (H_2O or O_2) could reduce the retrieval errors and increase the vertical resolution of the information, thanks to a better coverage of the atmospheric column by the increased number and better repartition of the weighting functions along the vertical.

The spectral features of the microwave range from 1 to 1000 GHz in terms of brightness temperatures (TB) measured from a nadir-viewing satellite are presented for six standard atmospheres, over ocean and land, in Figure 1. Note that we only consider protected spectral bands [*Mellinger*, 2007] (grey regions in Figure 1) in order to mitigate radio frequency interference (RFI).The spectrum is dominated by O_2 and H_2O lines, and the atmospheric opacity tends to increase with increasing frequency. Ozone lines are also present, but their strength is not sufficient to enable a good estimate of the ozone profiles from such observations. Except for the complex O_2 band around 60 GHz, the microwave spectrum is rather simple as compared to the IR spectrum, with most O_2 and H_2O lines isolated. With the microwave spectrum much less complicated than the IR one, we expect the number of useful hyperspectral channels to be more limited in the microwave than in the IR. As mentioned by *Blackwell et al.* [2011], hyperspectral in the microwave typically means a few hundred channels, not thousands of channels as in the IR. However, there should be no sharp cutoff as adding channels has an incremental effect with diminishing benefits as more channels are added.

Several studies already explored the potential of the higher spectral sampling in the microwave [*Lipton*, 2003; *Bauer and Di Michele*, 2007; *Blackwell et al.*, 2011], and the concept of a HYperSpectral Microwave Sensor (HYMS) was recently advocated by *Boukabara et al.* [2010]. *Blackwell et al.* [2011] analyze the performances of a hyperspectral instrument deployable on polar or geostationary satellites. They show that with 64 channels around the 118.75 GHz oxygen absorption line and 16 around the 183.31 GHz water vapor absorption line, the root-mean-square (RMS) errors in temperature profiling could be reduced by 0.5 K on average, compared to a traditional instrument such as AMSU-A and B, and that the RMS error in relative humidity is also reduced by

~5 % with respect to the a priori RMS. The improvements to the retrieval of the temperature and water vapor profiles are imputable partly to the high density of the weighting functions. *Boukabara and Garret* [2011] performed a pilot study highlighting the benefits of a HYMS for temperature profiling, especially under cloudy conditions. They simulated the performance of an instrument over ocean, with channels spanning over the 1–330 GHz portion of the microwave spectrum at a spectral resolution of 100 MHz. Reduction in the temperature profile error is evident when 100 channels are used in the retrieval, with a strong benefit under cloudy conditions where IR sounders are error prone at best and useless for opaque clouds.

Hyperspectral observations could also help mitigate RFI problems [*Gasiewski et al.*, 2002; *Misra et al.*, 2009]. Although regulated by the International Telecommunication Union, regulation of the use of the microwave frequencies RFI satellite passive microwave meteorological observations already suffers from contamination, even in protected bands (cf. Figure 1), and more and more emitters up to 100 GHz are emerging. There are two main types of RFI: pulse ultrawide bandwidth and continuous narrow bandwidth. Hyperspectral coverage of a given band can be very beneficial in mitigating the second type of RFI, in order to filter out the unphysical spectral spikes: the availability of multiple, correlated (i.e., partly sensitive to the same geophysical variable) channels can allow the rejection of individual contaminated channels without significant information content loss.

Recent technological developments make it now possible to plan hyperspectral instrumentation, in the microwave to submillimeter range, with high-quality measurements [*Hilliard et al.*, 2013]. So far, only a limited set of frequency channels have been considered in the microwave based on features within the microwave spectrum and historical evolution. Our objective is to investigate whether the microwave spectrum is sufficiently sampled by current and upcoming satellite instruments and whether new instruments with higher spectral resolution could improve the retrieval of thermodynamic profiles. For this purpose the retrieval accuracies of a hyperspectral conceptual instrument have been assessed in this study using a high number of selected channels among broad spectral bands along all major absorption features.

This paper analyses and quantifies the benefits of a HYMS instrument for atmospheric temperature and humidity profiling under clear-sky conditions. It is oriented toward the NWP community, and the methodology and assumptions will be as compatible as possible with the NWP practices. An information content analysis has been conducted, and special efforts were made to investigate the effects of errors in a priori information, instrument noise, and radiative transfer, for each configuration of the hyperspectral instrument (section 2). Two hyperspectral resolutions were considered (with a ratio of 10 between the two spectral resolutions). The performance of the hyperspectral instruments was systematically compared to the suite of the three microwave instruments to be on board the next generation of the European meteorological satellites (MetOp-SG) (section 3). So far, only frequencies up to 190 GHz are observed for operational weather forecasting, with the O_2 band around 60 GHz and the 183 GHz H_2O line of prime interest for temperature and water vapor profiling, respectively. MetOp-SG will provide measurements in the microwave and millimeter range, up to 664 GHz. This study considers all the relevant O_2 and H_2O lines and window channels, up to 874 GHz.

2. The Methodology and Tools
2.1. An Information Content Analysis
The standard information content analysis following *Rodgers* [2000] serves as the main tool to compare the different frequency channel selections and is briefly summarized here. By using Bayes' theorem, it is possible to estimate the distribution of errors of a one-dimensional variational retrieval scheme using satellite observations and a priori (i.e., background) information. The a posteriori probability of retrieval errors is characterized by its covariance matrix $\mathbf{A}$:

$$\mathbf{A}^{-1} = \mathbf{B}^{-1} + \mathbf{H}^T \mathbf{R}^{-1} \mathbf{H}, \tag{1}$$

where $\mathbf{H}^T$ is the transpose of the Jacobian matrix of the observation operator (i.e., the radiative transfer model), $\mathbf{B}$ is the error covariance matrix of the a priori state, and $\mathbf{R} = \mathbf{R}_\varepsilon + \mathbf{R}_f$ is the observation error covariance matrix including the instrumental noise ($\mathbf{R}_\varepsilon$) and the radiative transfer errors ($\mathbf{R}_f$).

Matrix $\mathbf{A}$ provides an estimate of the retrieval errors, without the need to perform the retrieval. The matrix $\mathbf{A}$ is very convenient to compare different instrument configurations and is commonly adopted in NWP centers. This estimation is based on the use of an a priori information and on the linearization of the radiative

transfer around the a priori. Three assumptions are used: (1) the random variables, i.e., a priori and observations errors, are Gaussian variables that can be characterized by covariance matrices **B** and **R**; (2) errors (instrumental, a priori information, radiative transfer, and linearization errors) are independent of each other; and (3) the radiative transfer is linear within the state space encompassing the a priori and the solution. In general, the radiative transfer is nonlinear with respect to humidity so using a linear information content approach could be problematic. However, if the a priori is close enough to the actual state vector, the linearization is satisfactory and the results of the information content are robust enough. In order to test the linearity and Gaussian character of equation (1), we have studied the linearization errors $\delta y = [RT(x) - RT(x_a) - K \cdot (x - x_a)]$, where RT is the forward radiatif transfer model, H is the RT Jacobian (estimated here at state x_a), and $x_a = x + e$ is the "analysis" that estimates state variable x with error e. It is then possible to compare distribution of δy in terms of Gaussianity and variance compared to the observation uncertainties (instrument and RT, i.e., matrix **R**). We have done these experiments for a limited number of situations x (about 20) because computations are rather costly. The Gaussian distribution is a good approximation of the δy distribution. Furthermore, the variance of δy is below 30% of the observation errors as specified in our studies in **R**.

In this paper, we consider the simultaneous retrieval of temperature and humidity. As a consequence, matrix **H** in equation (1) includes the Jacobians of both temperature and humidity. Considering both quantities have two opposing consequences for the retrieval error uncertainty estimation, on one hand, using the temperature/humidity dependence could facilitate the retrieval of the two profiles because the correlations between the temperature and humidity can be exploited by the retrieval. On the other hand, if uncertainty in parameters other than those to be retrieved is included in the analysis, this will increase retrieval uncertainty estimates in **A** (i.e., retrieval of humidity is more complex if temperature is not perfectly known a priori). Our test shows that the combined approach (simultaneous retrievals in equation (1)) provides higher errors in **A** than for the individual estimations. Again, this is to be expected; retrieval of humidity is more complex if there are uncertainties on temperature (and vice versa). the combined approach is more realistic and is used here. It is worth noting that our information content procedure is still not perfect as the linearization of the radiative transfer, more accurate for temperature than for humidity, and the description of the strong dependency of temperature and humidity might introduce uncertainties.

In the following sections the necessary ingredients for the information content analysis are described, following equation (1). The results of the information content analysis directly depend upon the assumptions made about the instrument noise figures in equation (1). As a consequence great care is taken in the estimation of these parameters to obtain realistic results. The strategy is to adopt hypotheses that are as compatible as possible with NWP center practices. The information content analysis needs to be performed on a large set of atmospheric situations, not on a few isolated profiles, to ensure more robust results. Therefore, a database of atmospheric profiles and related radiative transfer simulations is first built. A state-of-the-art atmospheric data set and the a priori information from the European Centre for Medium-Range Weather Forecasts (ECMWF) are selected. The results presented in this paper are obtained over ocean at nadir, but simulations have also been performed over land and for other angles (not shown). Only clear-sky cases are considered.

2.2. The Database of Atmospheric Profiles

The atmospheric profiles were extracted from the ECMWF profile databases [*Chevallier et al.*, 2006]. These databases were obtained from cycle 30R2 of the ECMWF forecasting system, with horizontal resolution of approximately 25 km on 91 pressure levels (http://research.metoffice.gov.uk/research/interproj/nwpsaf/rtm/profile_datasets.html). Only clear-sky scenes were selected, and three databases of 5000 profiles are available, one for the representation of temperature variability and similar ones for specific humidity and ozone. Data were selected only when coincident a priori covariance matrices **B** were available (see following section), which reduced the number of available profiles to 859 profiles from the temperature database, 344 from the humidity database and 786 from the ozone database.

The overall data set of 1989 profiles include a large range of temperature and humidity profiles, in particular many extreme cases. The data set was built with the intent of including profiles as diverse as possible. It does not represent the actual distribution of temperature, water vapor, and ozone profiles over the globe [*Aires and Prigent*, 2007], but it covers the whole variability of these profiles [*Chevallier et al.*, 2006; *Paul and Aires*, 2014].
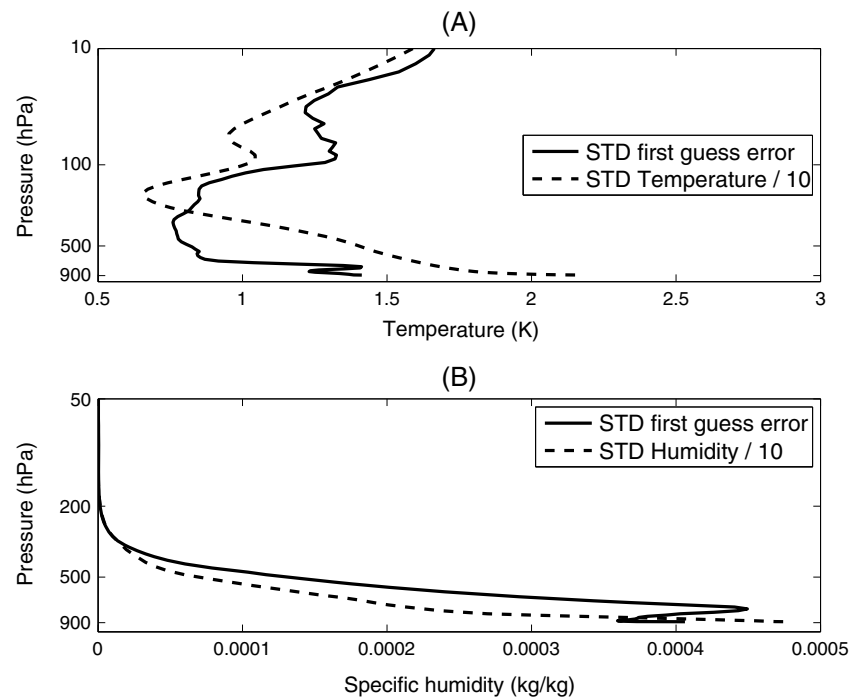
Figure 2. For (a) temperature and (b) specific humidity, the standard deviation (STD) of the a priori error and standard deviation (divided by a factor of 10) estimated over the full atmospheric data set.

The surface skin temperature is also provided with the ECMWF profiles. The surface emissivity is fixed at 0.6 over ocean. The emissivity is assumed to be error free and low; both of those assumptions lead to underestimation of retrieval uncertainty for temperature and humidity, relative to more general conditions.

2.3. The A Priori Error Covariance Matrices *B*

The information content analysis requires a priori error covariance matrices. These matrices represent the error covariance in the a priori atmospheric state, which, in the case of this work, is a model short-range forecast. In order to adapt as well as possible the NWP framework, *B* matrices have been derived from the ECMWF ensemble data assimilation system using the methodology described in *Holm and Kral* [2012]. The covariance matrices *B* result from the combination of the a priori error standard deviations and a vertical error correlation matrix.

The a priori error standard deviations are the same as those used to produce ECMWF analysis and vary in space and time because of their geographic variability and their flow dependency. The ensemble forecast dispersion is used as a proxy of the forecast errors. Their use to quantify the error of the a priori information should be considered with caution. Nevertheless, these dispersions are a good proxy for model forecast errors and they facilitate the assimilation of the satellite observations in the forecast model.

The vertical correlation matrices correspond to climatological averages calculated over a couple of seasons, over a 625 km resolution grid. Their main variations result mostly from geographical contrasts between ocean and land and from orography. Seasonal and diurnal variations are small compared to geographic variations. These matrices are separate for each variable and are available for temperature and a transformed variable for water vapor, which is introduced to reduce correlations with temperature and to produce errors that are more Gaussian [see *Holm and Kral*, 2012]. The transformation back to specific humidity introduces correlations with temperature. The main contributors to the correlations between temperature and specific humidity are complex and are due among others to condensation/evaporation processes and dynamic processes.

As indicated earlier, we are interested here in the retrieval of both temperature and humidity. For each 1989 atmospheric situation, the a priori covariance matrix **B** represents the error covariances of the a priori information for temperature and water vapor.

Figure 2 compares the standard deviations (STD) of the a priori errors and the variability estimated in the full atmospheric data set. The STD of the variability is divided by 10 to be comparable. The a priori appears to be

of very good quality; its errors are 10 times lower than the variability of temperature and humidity. Improving the initial information with the satellite observations is challenging with such a good a priori.

2.4. The Radiative Transfer Code

For each atmospheric situation, radiances are calculated with the radiative transfer code ARTS (Atmospheric Radiative Transfer Simulator [*Buehler et al.*, 2005; *Eriksson et al.*, 2011]). ARTS is an open-source, flexible model, primarily developed for the microwave region. ARTS has been compared and validated with other radiative transfer models [*Melsheimer et al.*, 2005; *Buehler et al.*, 2006].

Radiative transfer simulations have been performed for different incident angles and for both ocean and land. Here the ocean case at nadir is presented. ARTS can consider the Zeeman effect [*Larsson et al.*, 2014], but it has not been considered since this study focuses on NWP inside the troposphere and frequency ranges where the Zeeman effect is significant are avoided.

2.5. Selected Frequency Bands

To analyze the potential measurement performance in the 1 to 1000 GHz range, a number of frequency bands have been selected. These bands include channels located around absorption lines to allow the retrieval of vertical profiles of atmospheric O_2 and H_2O state parameters: around the 60 GHz O_2 band for temperature sounding; around the 118 GHz O_2 transition for temperature sounding; around the 183 GHz H_2O transition for water vapor sounding; around the 325 GHz H_2O transition for water vapor sounding; around the 420 GHz O_2 transition for temperature sounding; and around the 448 GHz H_2O transition for water vapor sounding.

Further, the selected bands include also window channels located between spectral lines to sense the lower part of the atmosphere and to account for the surface contribution. The characteristics of the sounding and window channels are presented in Table 1. Note that the O_2 band from 63.3 to 67.9 GHz is not in a protected region of the spectrum (Figure 1). However, the opacity in this band is expected to be large enough to prevent RFI from the ground but might be influenced by satellite-to-satellite communication.

An initial spectral resolution, "resolution 1," is first adopted as assumption for the hyperspectral instrument. For each of the nonwindow frequency bands, the resolution is selected according to the complexity of the lines. These frequency bands are divided in equal channels, with a width corresponding to "resolution 1." Table 1 gives the selected "resolution 1" for each frequency band. Furthermore, a factor of 10 is applied to "resolution 1" to obtain an improved spectral "resolution 2" (also indicated in Table 1)

For comparison purposes, the instruments to be on board MetOp-SG MicroWave Sounder (MWS), MicroWave Imager (MWI), and Ice Cloud Imager (ICI) have also been simulated. The characteristics of the MetOp-SG instruments are provided in Table 2. The instrument specifications have slightly changed since the beginning of this study, but these changes have not been considered here. The instrument noise figures indicated in the table correspond to the goal values: they are more stringent than the requirements imposed to the industry for the instrument development. As a consequence, they are indicative of optimum MetOp-SG instruments, with improved performances with respect to what will likely be available.

2.6. Jacobians

For cloud-free atmospheres, ARTS determines the temperature and humidity Jacobian matrices, **H**, in an analytical manner. The unit applied for Jacobians with respect to the temperature profile ($\partial T_b / \partial T_i$, where T_b is the brightness temperature and T_i is temperature at level i) is K/K. The unit applied for the Jacobians with respect to humidity ($\partial T_b / \partial q_i$, where q_i is the specific humidity at level i) is K/(kg/kg).

The mean of the temperature and humidity Jacobians for all the profiles is represented in Figure 3 for the HYMS bands. The O_2 band at 60 GHz is strongly sensitive to the temperature, as expected, and then less sensitive to water vapor. The sensitivity to water vapor is higher for the higher-frequency oxygen lines (118 and 420 GHz bands). The 183, 325, and 448 GHz bands provide information on temperature for lower atmospheric channels where they actually have a stronger Jacobian than the 118 GHz band. Note that these bands have also a strong sensitivity to humidity. With its complex and numerous absorption lines, the 60 GHz band provides a good sensitivity to the temperature all along the atmospheric profile, but the channel bandwidths in these frequencies need to be narrower to represent well the vertical resolution. Other broad spectral ranges show a significant sensitivity to the temperature (such as the 448 GHz line), but they are also very sensitive to the water vapor, making the information more ambiguous. However, it is important to note that Jacobians vary from one situation to another. Figure 4 represents the Jacobians for temperature and humidity for the 60 and

Table 1. Observation Errors for the HYMS Sounding and Window Channels[a]

Frequency Name (GHz)	Frequency Domain (GHz)	Instrument Noise (K)	RT Noise (K)	Bandwidth (MHz)	Number of Channels
HYMS-Sounder					
					Resolution 1
60 GHz	52.6–57.3 and 63.3–67.9	0.40	0.32	100	94
118 GHz	113.7–123.7	0.42	0.92	200	51
183 GHz	173.3–193.3	0.40	1.07	400	51
325 GHz	315.1–335.2	0.73	1.30	1000	21
420/448 GHz	416.8–432.8 and 440.0–456.0	0.93	1.47	1000	34
					Resolution 2
60 GHz	52.6–57.3 and 63.3–67.9	1.26	0.32	10	940
118 GHz	113.7–123.7	1.33	0.92	20	510
183 GHz	173.3–193.3	1.26	1.07	40	510
325 GHz	315.1–335.2	2.31	1.30	100	210
420/448 GHz	416.8–432.8 and 440.0–456.0	2.94	1.47	100	340
HYMS-Window					
6.92		0.13	1.93	350	1
10.65		0.25	1.93	100	1
15.37		0.21	1.92	150	1
18.70		0.19	1.91	200	1
21.30		0.20	1.86	200	1
22.35		0.17	1.84	290	1
23.80		0.14	1.86	400	1
31.65		0.18	1.88	300	1
36.50		0.10	1.86	1000	1
40.25		0.15	1.83	500	1
50.30		0.26	1.43	200	1
89.00		0.09	1.80	3000	1
101.00		0.12	1.79	2000	1
110.65		0.16	1.69	1300	1
150.00		0.13	1.72	3000	1
157.00		0.13	1.70	3000	1
165.50		0.13	1.62	3000	1
202.00		0.16	1.58	3000	1
207.00		0.16	1.61	3000	1
229.00		0.17	1.63	3000	1
237.00		0.18	1.60	3000	1
251.00		0.18	1.60	3000	1
298.00		0.21	1.58	3000	1
664.20		0.30	2.22	6000	1
874.00		0.39	2.92	6000	1

[a]The observation errors are divided in instrument and radiative transfer (RT) errors (see text for additional details). RT errors include both the surface and the atmospheric contributions.

the 183 GHz bands, for two contrasted atmospheric situations, one dry (specific humidity in atmospheric layers lower than $1 \cdot 10^{-3}$ kg/kg) and one wet (specific humidity in atmospheric layers higher than $2 \cdot 10^{-2}$ kg/kg). The impact on the Jacobians are relatively small in the 60 GHz band, except that the sensitivity to temperature appears to be higher for the lower part of the wet atmosphere. The Jacobians in the 183 GHz band are very different for the dry and wet cases. No sensitivity to temperature is observed for the dry case, but very high sensitivity is evident up to 300 hPa for the wet case. This figure illustrates the reasonably constant Jacobians in temperature-sounding channels, meaning that the retrieval using the O_2 bands is relatively linear. Contrarily,

Table 2. Observation Errors for the MetOp-SG Instruments (ICI, MWI, and MWS Instruments)[a]

ICI			MWI			MWS		
Frequency (GHz)	Instrument Noise (K)	RT Noise(K)	Frequency (GHz)	Instrument Noise (K)	RT Noise (K)	Frequency (GHz)	Instrument Noise (K)	RT Noise (K)
183.31±8.4	0.40	1.35	18.7	0.50	1.91	23.8	0.15	1.86
183.31±3.4	0.50	0.94	23.8	0.45	1.86	31.4	0.20	1.88
181.31±2.0	0.60	0.77	31.4	0.50	1.88	50.3	0.40	1.43
243.2±2.5	0.50	1.62	50.3	0.50	1.43	52.8	0.25	0.80
325.15±9.5	0.70	1.42	52.61	0.50	0.88	53.246±0.08	0.30	0.59
325.15±3.5	0.80	1.23	53.24	0.50	0.58	53.596±0.115	0.30	0.41
325.15±1.5	1.00	1.13	53.75	0.50	0.35	53.948±0.081	0.30	0.28
448±7.2	1.00	1.48	89.0	0.80	1.80	54.4	0.25	0.20
448±3.0	1.00	1.48	100.49	0.80	1.79	54.94	0.25	0.18
448±1.4	1.30	1.48	118.7503±4.0	0.70	1.39	55.5	0.30	0.18
664±4.2	1.00	2.21	118.7503±2.1	0.70	0.85	57.290344	0.30	0.19
			118.7503±1.4	0.70	0.39	57.290344±0.217	0.45	0.19
			118.7503±1.2	0.70	0.47	57290344±0.3222±0.048	0.45	0.18
			166.9	0.70	1.61	57.290344±0.3222±0.022	0.70	0.18
			183.31±8.4	0.60	1.35	89	0.25	1.80
			183.31±6.1	0.75	1.21	165.5	0.30	1.62
			183.31±4.9	0.75	1.10	183.311±7.0	0.40	1.27
			183.31±3.4	0.75	0.94	183.311±4.5	0.40	1.11
			183.31±2.0	1.00	0.77	183.311±3.0	0.60	0.89
						183.311±1.8	0.60	0.75
						183.311±1.0	0.75	0.69
						229	0.70	1.63

[a]The observation errors are divided in instrument and radiative transfer (RT) errors (see text for additional details).

the Jacobians in the H$_2$O bands are highly state dependent: the inversion process is nonlinear, and temperature and humidity information are mixed together. As a consequence, temperature information is necessary for the retrieval of humidity.

2.7. Instrument Noise, R_ε

In an information content analysis, the observation errors have to be specified. The instrument error, R_ε is the minimum detectable change in brightness temperature. It is given by the classical radiometric equation:

$$R_\varepsilon = (T_{\text{receiver}} + T_{\text{antenna}})/\sqrt{\text{Bandwidth} \cdot \tau}, \tag{2}$$

where T_{receiver} is the equivalent noise temperature of the receiver, T_{antenna} is the antenna temperature that is approximately equal to the scene brightness temperature, Bandwidth is the bandwidth of the receiver, and τ is the integration time. For simplicity sake, this radiometric equation neglects the fluctuation of the receiver gain as well as the calibration errors [*Hersman and Poe*, 1981]. The instrument noise levels used in this study for the HYMS concept rely on recent receiver noise specifications. From a collection of current state-of-the-art receivers, the following formula has been derived:

$$T_{\text{receiver}} = 4.5 \times F(\text{GHz}) + 30, \tag{3}$$

where the constants are in units of kelvins [*Aires et al.*, 2014]. An average T_{ant} of 270 K is assumed. The selected integration time (τ) is 20 ms for all channels, corresponding to the integration time for MWS on board MetOp-SG. Table 1 provides the noise assumptions for HYMS and Table 2 for MetOp-SG.

2.8. Radiative Transfer Errors, R_f

Radiative transfer (RT) errors are complex to estimate. Most information content studies simply provide a fixed error number that includes both the RT and the instrumental error, and the RT error covariance matrix is built with only diagonal elements. In this section, we present a simplified model for RT errors. It is based on
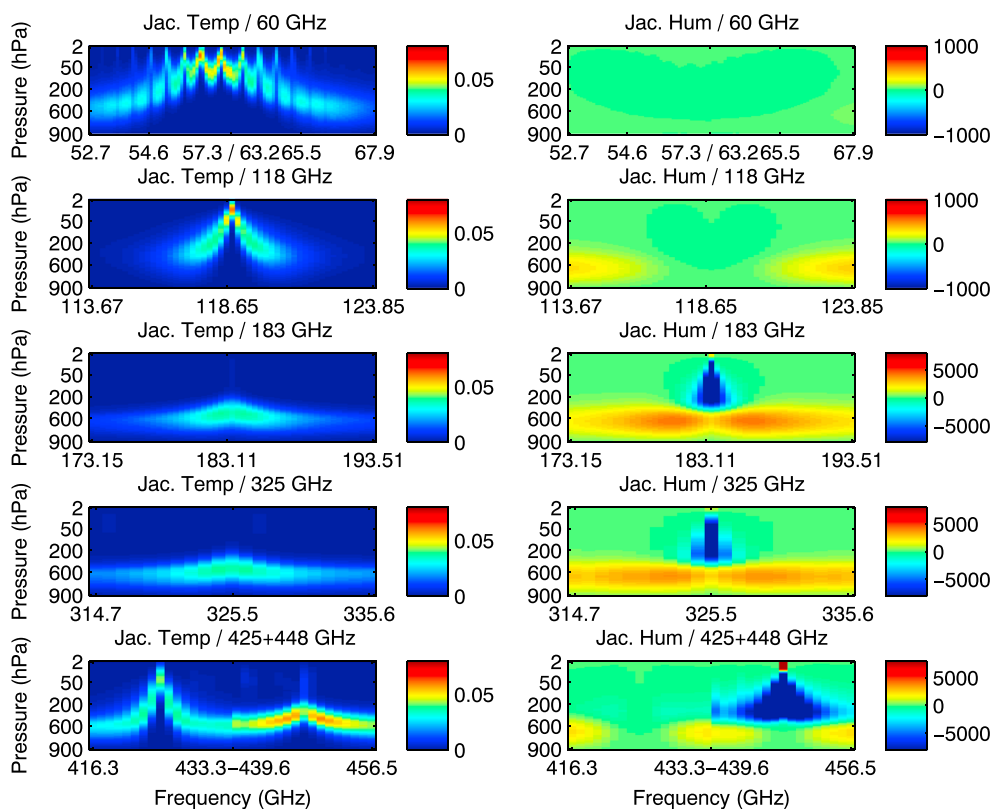
Figure 3. Mean Jacobians for (left) temperature in K/K and (right) humidity in K/kg/kg for the HYMS bands. Note that the humidity Jacobian color bar scale is not the same for all bands for illustrative purpose and that the 425 and 448 GHz bands are grouped on the same figure (with a discontinuity in frequency).

a Gaussian assumption too, but we will use more realistic error covariance matrices in order to facilitate the comparison between different spectral resolutions. The RT noise model described here is an attempt to better characterize these uncertainties, but it is still based on imperfect ad hoc assumptions. However, this is a first attempt and the community (NWP, RT modeling, and instrument specialists) should join forces to improve it in the future.

The first component to obtain a covariance matrix is the diagonal elements representing the variance of RT errors for each channel. The RT noise under clear-sky conditions includes contributions from the atmosphere and the surface. The clear-sky absorption/emission modeling error is assumed to increase linearly with frequencies, to account for the lack of experience with the frequencies above 200 GHz, as well as including noise to represent the increased potential of cloud contamination with frequencies.

However, the major source of radiative transfer noise is expected to come from the surface modeling. This noise is considered proportional to the emissivity error, $\delta emis$, estimated to be 0.01. The measurement can be written as (for specular cases)

$$T_b = T_d(1 - e)\tau + eT_s\tau + T_u, \tag{4}$$

where

T_d downwelling radiation;
e surface emissivity;
τ atmospheric transmission;
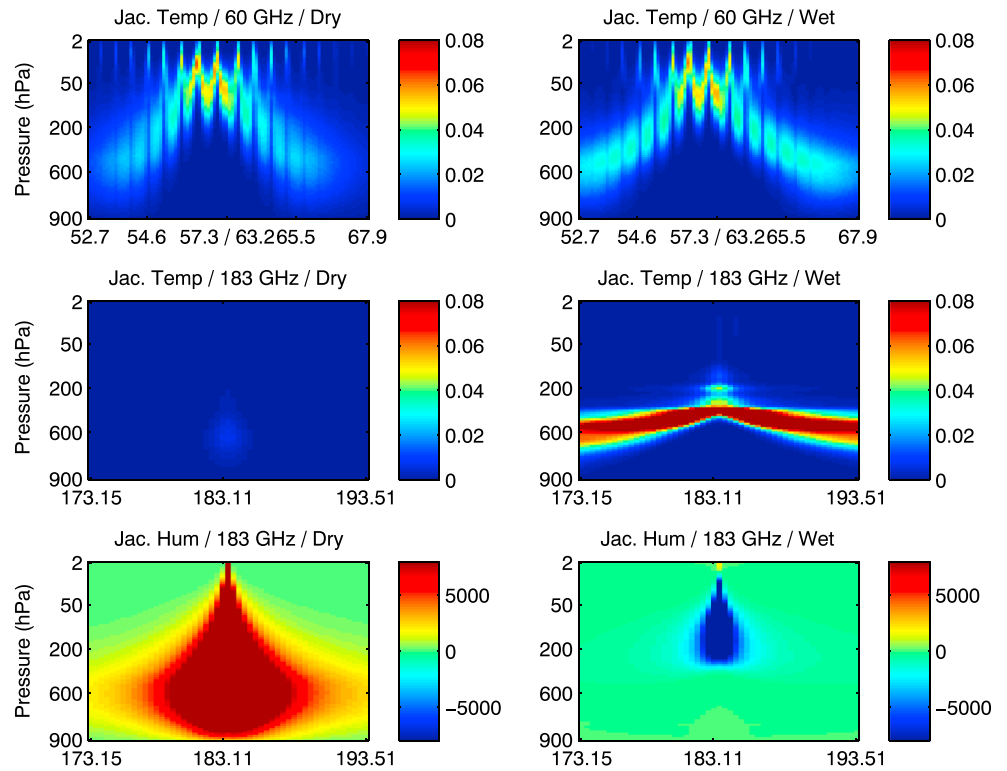T_s surface skin temperature;
T_u upwelling radiation.

Figure 4. (from top to bottom) Jacobians in temperature at 60 GHz, in temperature at 183 GHz, and in humidity at 183 GHz, for a very dry (left) and a wet (right) situation (see text).

For channels where the surface has a contribution, the atmospheric emission comes from the lowest kilometers and is approximately

$$T_u = T_d = (T_s - \Delta T)(1 - \tau), \tag{5}$$

where ΔT is a temperature difference (may vary from 5 to 30 K). This model for the tropospheric T_b is common for ground-based measurements. Putting this together,

$$dT_b/de = T_s \tau^2 + \Delta T(1 - \tau)\tau. \tag{6}$$

The second term is quite small, and we can simplify to

$$dT_b/de = T_s \tau^2. \tag{7}$$

Hence, the surface modeling error is situation dependent and it is set to $deT_s\tau^2$ where de is the error in surface emissivity e.

Figure 5a illustrates the radiative transfer noise, separated between the atmosphere (averaged over the atmospheric situations of the full data set) and the surface contributions. As expected, the noise is minimum in the absorption lines where the surface contribution is relatively small.

The second component of the RT error covariance matrix is the correlation matrix. The RT error specifications given in Table 1, and illustrated in Figure 5, are resolution independent. Indeed, the RT errors in ARTS (or in any other RT model) obtained in a channel are not dependent on the bandwidth of the channel. However, taking no correlation among channels close to each other would not be realistic. This would be artificially very beneficial to high spectral resolution: "n" multiple narrow channels close to each other would result in a RT error divided by $\sqrt{n}$, and this would be incorrect since each channel would have highly correlated systematic RT errors. As a consequence, instead of considering a diagonal covariance matrix $\mathbf{R}_f$, a nondiagonal matrix needs to be used to account for the correlation of errors among close channels. The correlation matrix
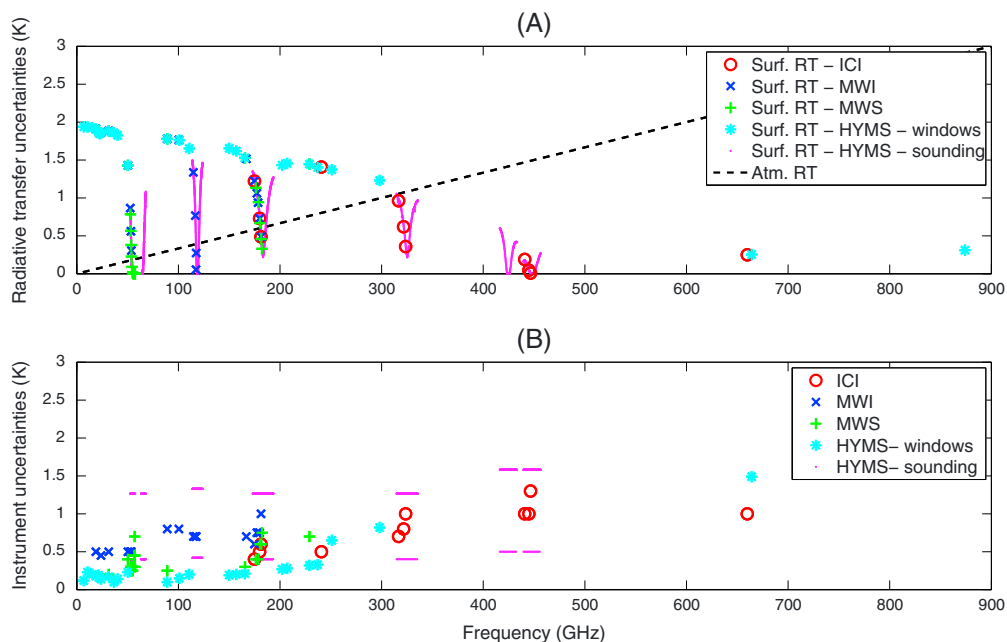
Figure 5. Observation noises for the MetOp-SG (ICI, MWI, and MWS) and the HYMS instruments, including (a) the radiative transfer errors for both the surface and atmospheric contributions separately (see text for more details) and (b) the instrument noises. The noise characteristics have been averaged over the whole atmospheric data set. For the hyperspectral channels, the instrument noise is represented in magenta for resolutions 1 (lower noise values) and 2 (higher noise values), i.e., the instrument error increases with better spectral resolution.

is built using a Gaussian shape truncated at two standard deviations to model the correlation dependence with frequency. By construction, these interchannel noise correlations are identical for the various spectral resolutions considered in this study. For one particular channel, the range of correlation is 1 GHz on each side of the channel.

Based on the noise standard deviations for each channel and on the correlation matrix, it is then possible to compute the overall RT error covariance matrix. Figure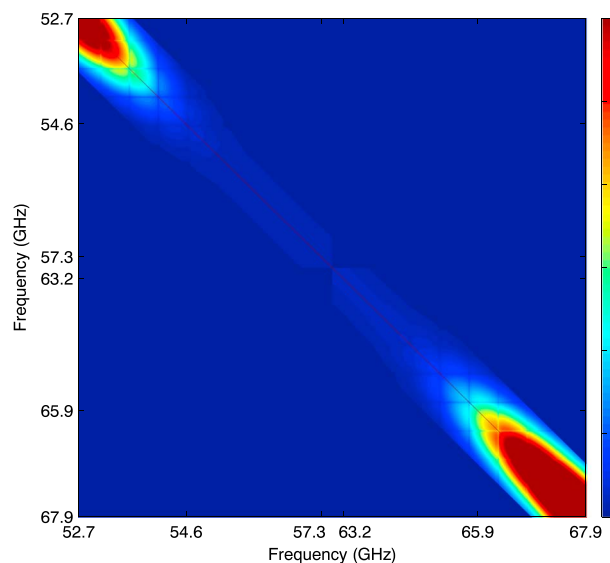 6 represents the observation error covariance matrix $\mathbf{R} = \mathbf{R}_\varepsilon + \mathbf{R}_f$ for the 60 GHz band at "resolution 2" (i.e., higher spectral resolution). It includes the RT error covariance matrix and the diagonal instrument error covariance matrix. The instrument errors are present on the diagonal only. The RT errors can be seen in the off-diagonal up to 1 GHz from the diagonal. Correlations are dependent on the frequency range only; they should appear in the figure on the full spectral range. However, the amplitude of RT noise being lower for the sounding channels than for the surface-sensitive channels, it can hardly be seen in the figure for the sounding channels. A fine squared structure can be noted that follows the pattern of the absorption lines.

Figure 6. Observation error covariance matrix including (1) the radiative transfer errors (surface and atmospheric contributions) plus (2) the instrumental errors in the diagonal only (see Table 1), for the 60 GHz band at "resolution 2."

2.9. Spectral Resolution Modulation

In order to test the sensitivity of a hyperspectral microwave instrument retrievals to the spectral resolution, we designed a
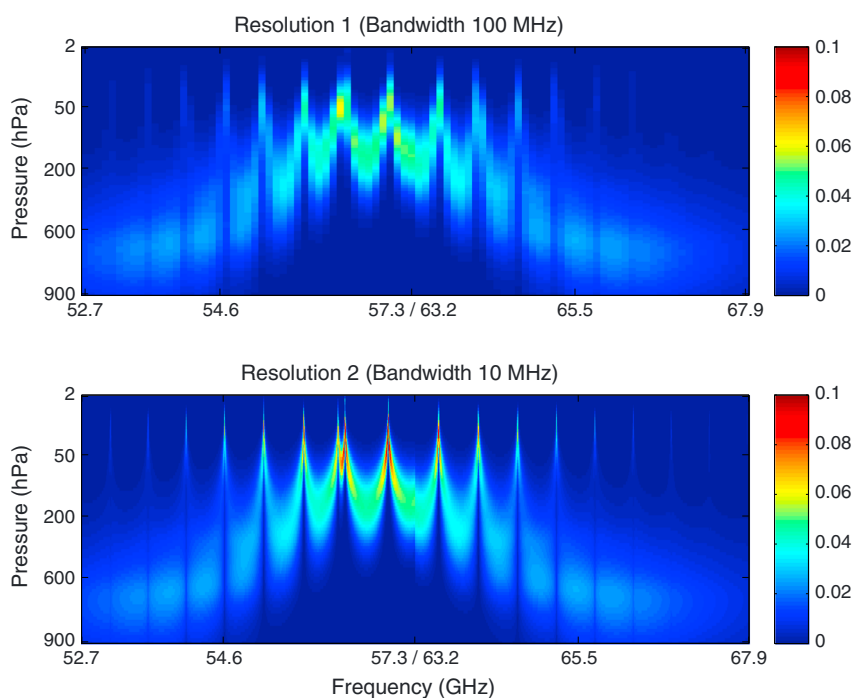
Figure 7. Jacobian in temperature (K/K) for the 60 GHz band, for the spectral (top) "resolution 1" (i.e., lower spectral resolution) and (bottom) "resolution 2" (higher spectral resolution). A discontinuity in these Jacobians can be noted: it corresponds to the gap between the two portions of the spectrum, from 52.6–57.3 GHz to 63.3–67.9 GHz.

procedure to build a database with multiple resolutions. The strategy is first to perform radiative transfer simulations with a very high spectral resolution (10 MHz in the 60 GHz band for "resolution 2") and then to degrade this very high resolution toward a coarser one by compositing the channels. Several channel bandwidths have been considered, but only two are presented here for simplicity of the presentation. The spectral averaging involves an approximation of Planck function linearity across the widest bands, but tests (not shown) indicate that this is a very good approximation. The noise of a channel decreases proportionally with the square root of its bandwidth; see equation (2). The resulting coarser spectral resolution Jacobians are also the average of the higher-resolution Jacobians.

2.10. Impact of the Spectral Resolution on the Jacobians

Figure 7 represents the temperature Jacobians in the 60 GHz band for spectral resolutions 1 and 2. The amplitude of the Jacobians is lower for the coarser spectral resolution. The absorption lines are thinner and sound higher in the vertical with the highest spectral resolution 2.

Figure 8 is the equivalent of Figure 7, but instead of a 2-D representation, each channel is represented by a Jacobian profile. As expected, with a high spectral resolution ("resolution 2"), some channels sound high in the atmosphere: this is explained by the very thin and complex line structure in the 60 GHz band that can only be captured by the high spectral resolution. Note that Jacobian values in upper layers need to be considered with caution since the Zeeman effect was not taken into account in the radiative transfer calculations.

The effect of the spectral resolution is not only on the altitude of the peak of the Jacobian. It also affects the amplitude as well as the width of the Jacobians. The amplitude is higher at the finer spectral resolution. The width at midheight (WMH) of the temperature Jacobians (expressed in number of atmospheric layers) has been estimated for the 60 GHz band, for the two spectral resolutions. It is only the number of atmospheric layers between (1) the higher atmospheric layer with Jacobian value equal to half the maximum of the Jacobian and (2) the lower layer with Jacobian value again equal to half the maximum of the Jacobian. The mean WMH for lower sounding channels is about the same for the two resolutions (∼30 layers), meaning that the spectral resolution is not impacting the Jacobians near the surface. In contrast, for higher sounding channels (e.g., peaking between 100 and 50 hPa) the averaged WMH is much lower for resolution 2 (19 layers) than for resolution 1 (26 layers). In conclusion, in the lower atmosphere, the change in the Jacobians should not directly
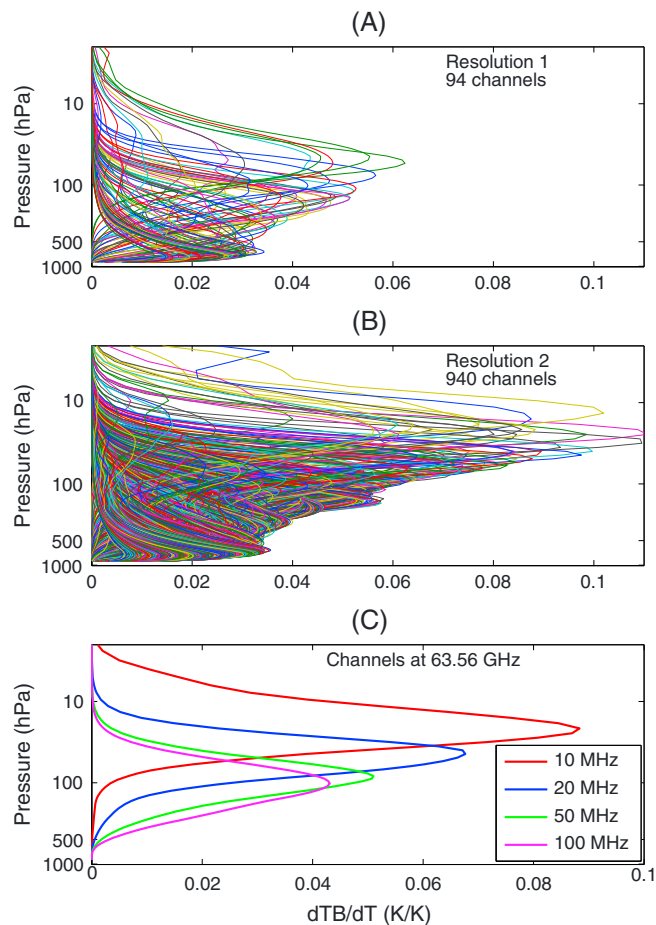
Figure 8. Jacobians in temperature (K/K) in the 60 GHz band (a) for resolution 1 and (b) for resolution 2. (c) Jacobians at 63.56 GHz for resolutions 1 (100 MHz) and 2 (10 MHz) and two other intermediate resolutions (20 and 50 MHz).

affect the vertical resolution of the retrieval whereas at higher altitude, the higher the spectral resolution is, the thinner the Jacobians are and, as a consequence, the better the vertical resolution becomes.

3. The Results of the Information Content Analysis

Following a common practice, the retrieval statistics are provided in terms of improvement of the a priori errors. An improvement of 10% means that the satellite observations decrease the uncertainty with 10% compared to a priori. Figure 9 represents the estimation of the retrieval statistics using equation (1) for temperature (a) and water vapor (b). The percent change was computed for each profile and then averaged over the full database. The initial hyperspectral instrument with resolution 1 (HYMS/Res. 1) can provide a significant improvement in the lower layers in temperature (up to ~10%) and in water vapor (up to ~30%). Maximum improvement in temperature is only about 10%, but note that in this study, the a priori errors (section 2.3) are rather optimistic.

Tests have been made to check the validity of the information content analysis for the retrieval of water vapor. The Gaussian hypothesis and the nonlinear behavior of the RT could be a limitation. Results show that the Gaussian approximation of the errors is satisfactory and that variance of errors due to the linearization are below 30% of the observations errors as specified in this study (not shown).

3.1. Comparison With the MetOp-SG Microwave Instruments

Similar error estimates are conducted for the three microwave MetOp-SG instruments, separately and then jointly (Figure 9). As expected, the sounding instrument MWS performs better than the imaging ones (ICI and MWI), for both temperature and water vapor profiling, except for humidity where ICI has a higher improvement rate than MWS at pressures below 600 hPa, thanks to its high-frequency channels. Their combined use
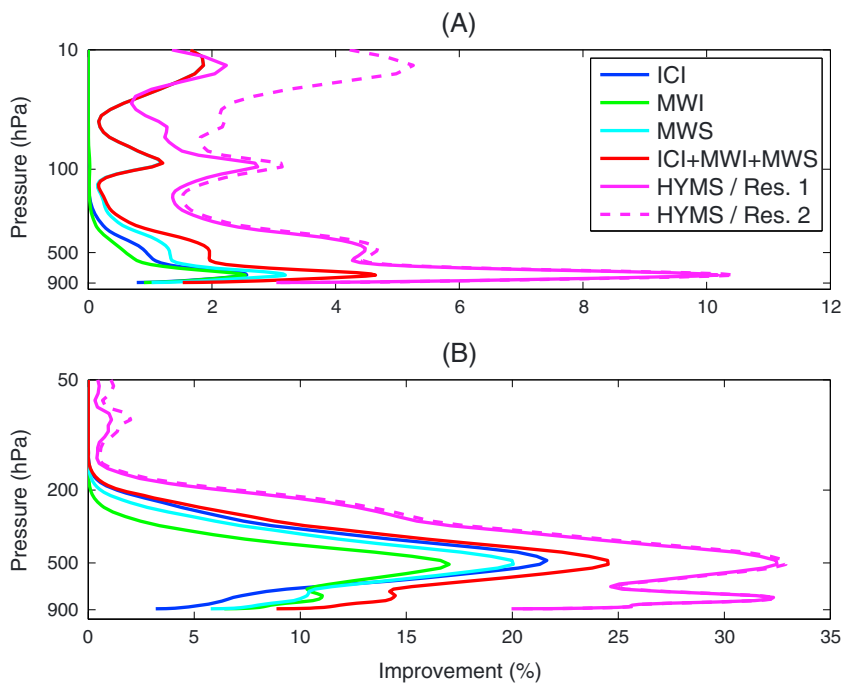
Figure 9. Estimation of the retrieval statistics in terms of relative improvement in percent to the a priori. Statistics are provided (a) for temperature and (b) for humidity (bottom), for the HYMS instrument with spectral resolutions 1 (lower spectral resolution, solid line) and 2 (higher spectral resolution, dashed line) as well as for the MetOp-SG microwave instruments, separately and jointly.

(ICI + MWI + MWS) provides a noticeable improvement as compared to MWS. This advocates for the synergistic use of all three instruments for optimal benefit retrievals. Note, however, that this simulation neglected factors that would degrade practical retrievals using a combination of the sensors, such as differences in field of view and view angle. The improvements of the HYMS instrument (Res. 1) compared to the MetOp-SG instrument combination are more than double at pressure over 100 hPa for temperature, and are also significant for humidity, at pressures over 250 hPa. Although the spectral resolution for this HYMS configuration is not very high, these results show that a hyperspectral microwave instrument would provide better results than the currently planed MetOp-SG microwave suite. Considering the findings in section 2.10, the improvement in profiling error statistics in the lower layers is not due to the decreasing width of the Jacobian with decreasing bandwidth. It is due mostly to the addition of the channels that provides a decreasing noise, although the noise in these channels are not completely independent (see section 2.8). Note that suppressing the noise correlation between the channels would artificially increase the benefit of the hyperspectral instrument (not shown).

3.2. Sensitivity to the Hyperspectral Resolution

The sensitivity to spectral resolution exists for temperature only and only in the upper atmosphere above 100 hPa. This is expected as the channels sounding in this region correspond to fine spectral structure in the O_2 band around 60 GHz, which can only be captured with high spectral resolution (see sections 2.9 and 2.10). An optimum could be found in the spectral resolution of the hyperspectral instrument since the retrieval uncertainty does not keep decreasing significantly with increasing spectral resolution [*Lipton*, 2003]. Note that the optimum spectral resolution will strongly depend upon the assumption on the instrument noise as well as on the error covariance in the radiative transfer noise.

3.3. Sensitivity to the Frequency Bands With Hyperspectral Resolution

For an optimum design of future microwave instruments for NWP application, it might not be necessary to have hyperspectral observations in all frequency bands but only for one or two bands. The O_2 band around 60 GHz is a natural candidate, given its impact on the temperature profiling and the complexity of the lines, as compared to the other bands. The 183 GHz can also be considered. Experiments (not shown here) indicate that these two bands contain more information than other bands for the clear-sky case. Under cloudy conditions, a sensitivity analysis will have to be conducted to check if the conclusions apply in this case, too.
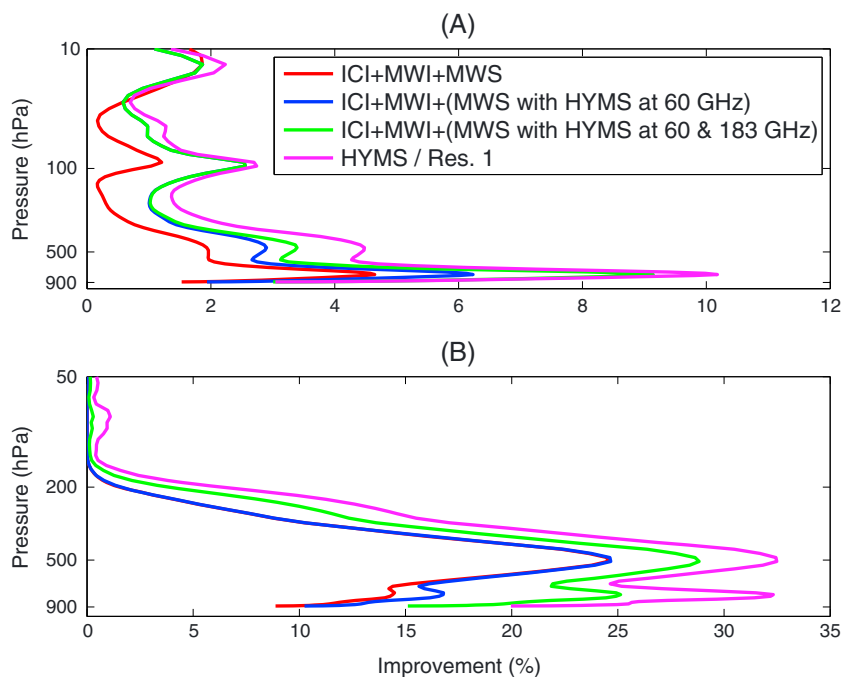
Figure 10. Estimation of the retrieval statistics in terms of a priori improvement in percent. Statistics are provided (a) for temperature and (b) for humidity, for (1) the MetOp-SG instruments, (2) a MetOp-SG configuration where the 60 GHz channels are replaced by those of HYMS, (3) a configuration where both 60 and 183 GHz channels are replaced, and (4) the full HYMS instrument at resolution 1.

Estimation of the retrieval statistics in terms of a priori improvement are provided for temperature and humidity (Figure 10) for (1) the MetOp-SG instruments (red), (2) a MetOp-SG configuration where the 60 GHz channels are replaced by those of HYMS, (3) a configuration where both 60 and 183 GHz channels are replaced, and (4) the full HYMS instrument at resolution 1. The impact of the 60 GHz high spectral resolution is clear for the temperature retrieval up to 40 hPa. The addition of the hyperspectral resolution at 183 GHz is beneficial for both water vapor and temperature sounding, leading to those that tend toward the performances of the full hyperspectral instrument.

A parallel study was conducted *Mahfouf et al.* [2015] to show that a channel selection among the resolution 1 instrument was possible and could obtain similar retrieval statistics with about half of the channels (110 selected channels among the 276 channels of HYMS/Res. 1). Furthermore, the Information Content (IC) could be numerically sensitive to the number of channels used in equation (1), and the comparison of the retrieval statistics for resolutions 1 and 2 could not be robust. In order to check this aspect, we performed the IC analysis with 2510 + 25 inputs (the higher resolution 2 configuration) even for the lower resolution 1 but using for the additional channels random Gaussian noise. Results (not shown) are identical, which shows that the IC is not artificially sensitive to the number of channels but rather to the information conveyed by the inputs.

3.4. Sensitivity to Instrument Noise
The results from the previous sections are encouraging concerning the interest of hyperspectral observations. The hyperspectral observing system improves the retrieval as compared to carefully selected channels as in MetOp-SG, despite the degradation of the noise characteristics of the instrument channels with decreasing spectral bandwidth (equation (1)). However, building a high spectral resolution instrument with an instrument noise following $\sqrt{\text{Bandwidth}}$ can be too optimistic for very high spectral resolutions, and additional noise might have to be considered related to the back end processing. It is therefore important to quantify here the sensitivity of the retrieval quality to the noise assumptions. Figure 11 represents the improvements of the retrieval for both temperature and humidity compared to the a priori information when noise on resolution 1 case is increased by 20, 40, and 60%. For all cases, the performance of the HYMS resolution 1 is much higher than that of the MetOp-SG microwave instrument combination. This shows that a high-resolution instrument is beneficial even if the instrument noise characteristics are degraded with increased spectral resolution. The
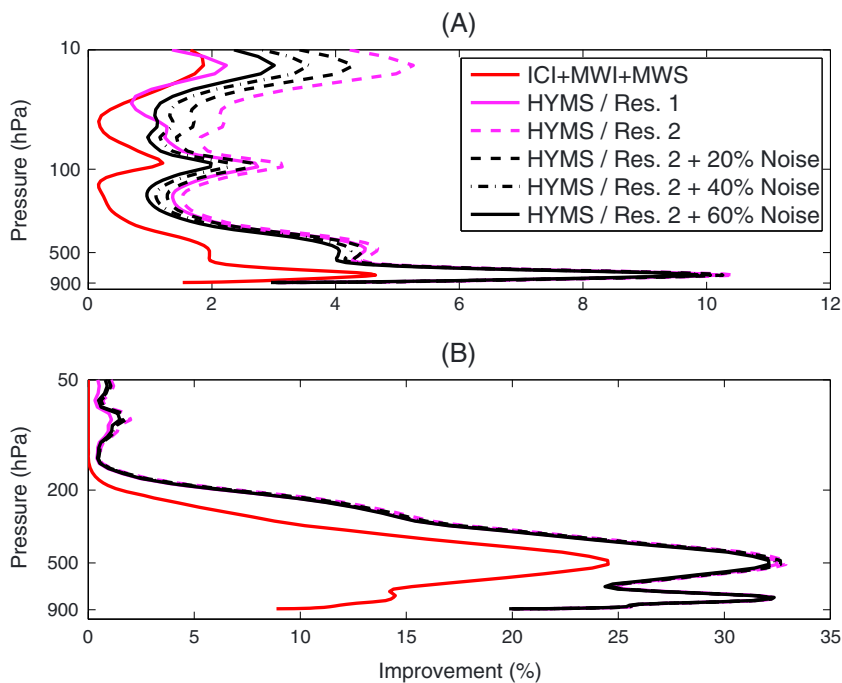
Figure 11. Impact of the noise level on the improvement in (a) temperature and (b) water vapor, as compared to the a priori information. Improvements are represented for MetOp-SG, for HYMS resolution 1, and for HYMS resolution 2 with various levels of instrument noise (+20, +40, and +60%).

impact of instrumental noise is negligible in the lower atmospheric layers since the RT uncertainties are the dominant component in the observation noises (see Table 2 and Figure 5). Very limited impact is noticeable for humidity profiling since redundant observations compensate largely for the increased errors.

4. Conclusions

The objective of this study was to analyze the benefits of a hyperspectral instrument in the microwave (HYMS) for temperature and water vapor profiling under clear-sky conditions. An extensive database of microwave simulations (radiances and associated Jacobians) has been created, from 6 to 900 GHz. An information content analysis has been developed and applied to this database to study different HYMS configurations. It involves realistic a priori (background) information and observation noise (from the radiative transfer and the instruments). The results are presented over ocean at nadir. Similar conclusions were drawn for other incident angles and over land (not shown). The results show the benefit of the hyperspectral information on the retrieval of temperature and water vapor as compared to the microwave/millimeter wave instruments planed for the MetOp-SG mission. Improvement compared to the a priori information on temperature goes from 2% to 10%, depending on the atmospheric layers, and is more than twice what will be obtained with MetOp-SG. Improvements for humidity sounding can reach 30%, a significant benefit as compared to MetOp-SG results especially up to 500 hPa. These are very positive results considering the very high quality of the a priori information. The results are not very sensitive to the instrument noises, under our assumptions.

Instrumental noise degrades with increasing spectral resolution, and so the multiplication of channels does not play a direct role (i.e., better signal-to-noise ratio) on the retrieval statistics: the bandwidth and the instrument noise compensate each other. However, the impact of the hyperspectral observations can take two other forms. First, benefits can arise when the decrease of the bandwidth results in a more vertically localized Jacobian, allowing for a better vertical description of the profiles. This occurs for the 60 GHz band for temperature, where the Jacobians are sensitive to the spectral resolution. For the other bands, no Jacobian sensitivity to spectral resolution was observed. Second, improvements arise when noises among channels have some degree of independence. In many bands, the radiative transfer errors dominate the instrumental noises. These RT errors are not entirely correlated to each other. The multiplication of channels in this case decreases the RT errors and thus improve the retrieval accuracies. This means that even lower

information bands could be beneficial to an observing system (e.g., the 118 or 420 GHz bands could still help the 60 GHz band) due to their "denoising" synergy [*Aires*, 2011]. Hyperspectral instruments can benefit from the combined effect of these two processes, even under the clear-sky conditions.

In the clear-sky case, the retrieval of temperature and humidity using infrared measurements from IASI has proven to be a very significant contribution to NWP forecast centers. Using the microwave observations in the clear-sky case could be questioned in this context. However, it has been shown in the past that even in the clear-sky case, a MW instrument such as AMSU can still be used in addition to IASI, and the IR/MW data fusion synergy is strong and beneficial: For temperature, adding the microwave to the infrared reduces by up to 20% the RMS error. For humidity, RMS errors are also significantly reduced by 5 to 10% [*Aires*, 2011; *Aires et al.*, 2011, 2012]. Therefore, an improvement in the MW instrumentation should still benefit NWP centers. Furthermore, microwave observations are less sensitive to thin clouds such as cirrus. These clouds might be transparent for HYMS, so it could be considered to be clear-sky case but cloudy for infrared. HYMS could then be very beneficial for these cases. Another major application of the hyperspectral measurements is the mitigation of radio frequency interferences, but the present study does not quantify this interest.

Hyperspectral observations in the microwave and millimeter domains are now technologically possible, and this potential opens new exciting possibilities. A significant improvement in the NWP capabilities can be expected, even under clear conditions, even if it is not as important to what has been observed with the advent of the infrared hyperspectral information. In a companion paper [*Mahfouf et al.*, 2015], it is shown that it is possible to select a subset of channels among the large number of channels of a HYMS instrument concept in order to reduce the computational burden in NWP operations while preserving the improvement to current or planned instruments.

The analysis of the benefit of hyperspectral microwave information for cloudy situations will be the object of the next study. Radiative transfer calculation will be performed over a variety of cloudy and precipitating situations, and an information content analysis will quantify the impact of the hyperspectral observations on the retrieval of the temperature and water vapor profiles under cloudy conditions as well as on the profiling of precipitation (liquid or solid) and cloud liquid water and ice.

References

Aires, F. (2011), Measure and exploitation of multisensor and multiwavelength synergy for remote sensing: 1. Theoretical considerations, *J. Geophys. Res.*, *116*, D02301, doi:10.1029/2010JD014701.

Aires, F., and C. Prigent (2007), Sampling techniques in high-dimensional spaces for the development of satellite remote sensing database, *J. Geophys. Res.*, *112*, D20301, doi:10.1029/2007JD008391.

Aires, F., M. Paul, C. Prigent, B. Rommen, and M. Bouvet (2011), Measure and exploitation of multi-sensor and multi-wavelength synergy for remote sensing: Part II—An application for the retrieval of atmospheric temperature and water vapour from METOP, *J. Geophys. Res.*, *116*, D02302, doi:10.1029/2010JD014702.

Aires, F., O. AZNAY, C. Prigent, M. Paul, and F. Bernardo (2012), Synergistic multi-wavelength remote sensing versus a posteriori combination of retrieved products: Application for the retrieval of atmospheric profiles using MetOp-A, *J. Geophys. Res.*, *117*, D18304, doi:10.1029/2011JD017188.

Aires, F., C. Prigent, J.-F. Mahfouf, E. Orlandi, and M. Milz (2014), WorkPackage 2—Clear sky analysis, *Tech. Rep.*, ESA, Estec, Netherlands.

Bauer, P., and S. Di Michele (2007), Study on definition of mission requirements for a post-EPS microwave radiometer for cloud and precipitation observation, *EUMETSAT Cntract EUM/CO/O6/1510/PS*, ECMWF, Reading, U. K.

Bauer, P., A. J. Geer, P. Lopez, and D. Salmond (2010), Direct 4D-Var assimilation of all-sky radiances. Part I: Implementation, *Tech. Rep.*, European Centre for Medium–Range Weather Forecasts, Reading, U. K.

Blackwell, W. J., L. J. Bickmeier, R. V. Leslie, M. L. Pieper, J. E. Samra, C. Surussavadee, and C. A. Upham (2011), Hyperspectral microwave atmospheric sounding, *IEEE Trans. Geosci. Remote Sens.*, *49*(1), 128–142, doi:10.1109/TGRS.2010.2052260.

Boukabara, S. A., and K. Garret (2011), Benefits of a hyperspectral microwave sensor, *IEEE Sens. Proc.*, pp. 1881–1884, doi:10.1109/ICSENS.2011.6127357.

Boukabara, S. A., K. Garret, P. VanDelst, D. Groff, Q. Liu, S. A. Clough, F. Eng, R. Ferraro, and T. Kleespies (2010), Scientific arguments for a hyperspectral microwave sensor (HyMS), paper presented at EUMETSAT Meteorological Satellite Conference, Cordoba, Spain.

Buehler, S. A., P. Eriksson, T. Kuhn, A. von Engeln, and C. Verdes (2005), ARTS, the atmospheric radiative transfer simulator, *J. Quant. Spectrosc. Radiat. Transfer*, *91*(1), 65–93, doi:10.1016/j.jqsrt.2004.05.051.

Buehler, S. A., N. Courcoux, and V. O. John (2006), Radiative transfer calculations for a passive microwave satellite sensor: Comparing a fast model and a line-by-line model, *J. Geophys. Res.*, *111*, D20304, doi:10.1029/2005JD006552.

Cardinali, C. (2009), Forecast sensitivity to observation (FSO) as a diagnostic tool, *Tech. Rep.*, European Centre for Medium–Range Weather Forecasts, Reading, U. K.

Chevallier, F., S. Di Michele, and A. P. McNally (2006), *Diverse Profile Datasets From the ECMWF 91-Level Short-Range Forecasts*, Eur. Cent. for Medium-Range Weather Forecasts, Reading, U. K.

Dee, D., et al. (2011), The ERA-Interim reanalysis: Configuration and performance of the data assimilation system, *Q. J. R. Meteorolog. Soc.*, *137*, 553–597.

Eriksson, P., S. A. Buehler, C. P. Davis, C. Emde, and O. Lemke (2011), ARTS, the atmospheric radiative transfer simulator, version 2, *J. Quant. Spectrosc. Radiat. Transfer*, *112*(10), 1551–1558, doi:10.1016/j.jqsrt.2011.03.001.

Gasiewski, A. J., M. Klein, A. Yevgrafov, and V. Leuski (2002), Interference mitigation in passive microwave radiometry, in *Proc. IGARSS'02, 2002 IEEE International Geoscience and Remote Sensing Symposium Toronto, ON, Canada, 24–28 June*, vol. 3, pp. 1682–1684, IEEE, Piscataway, N. J.

Geer, A. J. (2013), All-sky assimilation: Better snow-scattering radiative transfer and addition of SSMIS humidity sounding channels, *Tech. Rep.*, European Centre for Medium–range Weather Forecasts (ECMWF), Reading, U. K.

Hersman, M. S., and G. A. Poe (1981), Sensitivity of the total power radiometer with periodic absolute calibration, *IEEE Trans. Microwave Theory Tech.*, *29*(1), 32–40, doi:10.1109/TMTT.1981.1130283.

Hilliard, L., P. Racette, W. Blackwell, C. Galbraith, and E. Thompson (2013), Hyperspectral Microwave Atmospheric Sounder (HyMAS) architecture and design accommodations, in *Aerospace Conference, 2013 IEEE Aerospace Conference, Big Sky, Mont., 2–9, March*, pp. 1–11, IEEE, doi:10.1109/AERO.2013.6496895.

Holm, E. V., and T. Kral (2012), Flow-dependent, geographically varying background error covariance for 1D-var applications in MTG-IRS L2 processing, *Tech. Rep.*, European Centre for Medium–Range Weather Forecasts (ECMWF), Reading, U. K.

Larsson, R., S. A. Buehler, P. Eriksson, and J. Mendrok (2014), A treatment of the Zeeman effect using Stokes formalism and its implementation in the Atmospheric Radiative Transfer Simulator (ARTS), *J. Quant. Spectrosc. Radiat. Transfer*, *133*, 445–453, doi:10.1016/j.jqsrt.2013.09.006.

Lipton, A. E. (2003), Satellite sounding channel optimization in the microwave spectrum, *IEEE Trans. Geosci. Remote Sens.*, *41*(4), 761–781, doi:10.1109/TGRS.2003.810926.

Lorenc, A. C., and R. T. Marriott (2014), Forecast sensitivity to observations in the Met Office Global numerical weather prediction system, *Q. J. R. Meteorolog. Soc.*, *140*(678), 209–224, doi:10.1002/qj.2122.

Mahfouf, J.-F., C. Birman, F. Aires, C. Prigent, E. Orlandi, and M. Milz (2015), Information content on temperature and water vapour from a hyper-spectral microwave sensor, *Q. J. R. Meteorol. Soc.*, doi:10.1002/qj.2608.

Mellinger (2007), *Handbook of Frequency Allocations and Spectrum Protection for Scientific Uses, Panel on Frequency Allocations and Spectrum Protection for Scientific Uses*, Natl. Academies Press, Washington, D. C.

Melsheimer, C., et al. (2005), Intercomparison of general purpose clear sky atmospheric radiative transfer models for the millimeter/submillimeter spectral range, *Radio Sci.*, *40*, RS1007, doi:10.1029/2004RS003110.

Misra, S., P. N. Mohammed, B. Güner, C. S. Ruf, J. R. Piepmeier, and J. T. Johnson (2009), Microwave radiometer radio-frequency interference detection algorithms: A comparative study, *IEEE Trans. Geosci. Remote Sens.*, *47*(11), 3742–3754, doi:10.1109/TGRS.2009.2031104.

Paul, M., and F. Aires (2014), Using Shannon's entropy to sample heterogeneous and high-dimensional atmospheric datasets, *Q. J. R. Meteorol. Soc.*, *141*, 469–476, doi:10.1002/qj.2367.

Radnoti, G., P. Bauer, A. McNally, C. Cardinali, S. Healy, and P. de Rosnay (2010), ECMWF study on the impact of future developments of the space-based observing system on numerical weather prediction, *Tech. Rep.*, ECMWF, Reading, U. K.

Rodgers, C. D. (2000), Inverse methods for atmospheric sounding—Theory and practice, *Ser. on Atmos. Oceanic and Planet. Phys.*, World Sci., Singapore, doi:10.1142/9789812813718.